INTERNATIONAL ATOMIC ENERGY AGENCY
UNITED NATIONS EDUCATIONAL, SCIENTIFIC AND CULTURAL ORGANIZATION
INTERNATIONAL CENTRE FOR THEORETICAL PHYSICS
I.C.T.P., P.O. BOX 586, 34100 TRIESTE, ITALY, CABLE CENTRATOM TRIESTE

H4.SMR/449-39

WINTER COLLEGE ON
HIGH RESOLUTION SPECTROSCOPY

(8 January - 2 February 1990)

INSTABILITIES AND CHAOS IN LASERS: INTRODUCTION TO HYPERCHAOS

T. Arecchi

(lecture given by R. Meucci)

Istituto Nazionale di Ottica
Firenze 50125 Arcetri
Italy

Instabilities and Chaos in Lasers: Introduction to Hyperchaos.

F. T. ARECCHI

Istituto Nazionale di Ottica
Dipartimento di Fisica dell'Università - Firenze, Italia

1. – Introduction.

Quantum optics from its beginning was considered as the physics of coherent and intrinsically stable radiation sources. Lamb's semi-classical theory [1] showed the role of the e.m. field in the cavity in ordering the phases of the induced atomic dipoles, thus giving rise to a macroscopic polarization and making it possible a description in terms of very few collective variables. In the case of a single-mode laser and a homogeneous gain line this meant just five coupled degrees of freedom, namely, a complex field amplitude E, a complex polarization P and a population inversion N. A corresponding quantum theory, even for the simplest model laser (the so-called Dicke model, that is, a discrete collection of modes interacting with a finite number of two-level atoms), does not lead to a closed set of equations, however the interaction with other degrees of freedom acting as a thermal bath (atomic collisions, thermal radiation) provides truncation of high-order terms in the atom-field interaction [2-4]. The problem may be reduced to five coupled equations (the so-called Maxwell-Bloch equations), but now they are affected by noise sources to account for the coupling with the thermal bath [5]. These being stochastic, or Langevin, equations, the corresponding solution in closed form refers to a suitable weight function or phase-space density. Anyway the average motion matches the semi-classical one, and fluctuations play a negligible role if one excludes the bifurcation points where there are changes of stability in the stationary branches. Leaving out the peculiar statistical phenomena which characterize the threshold points and which suggested a formal analogy with thermodynamic phase transitions [6], the main point of interest is that a single-mode laser provides a highly stable or coherent radiation field.

From the point of view of the associated information, the standard interferometric or spectroscopic measurements of classical optics, relying on average field values or on their first-order correlation functions, are insufficient. In

order to characterize the statistical features of quantum optics, it was necessary to make extensive use of photon statistics [7, 8].

As discussed in detail in sect. 2, coherence is equivalent to having a stable fixed-point attractor and this does not depend on the details of the nonlinear coupling, but on the number of relevant degrees of freedom. Since such a number depends on the time scales on which the output field is observed, coherence becomes a question of time scales. This is the reason why for some lasers coherence is a robust quality, persistent even in the presence of strong perturbations, whereas in other cases coherence is easily destroyed by the manipulations common in the laboratory use of lasers, such as modulation, feedback or injection from another laser.

Here we review instabilities and chaos in active quantum optics. Section 2 is a general presentation of low-dimensional chaos in lasers, including the description of the relevant measurements upon which any assessment on chaos has to rely. Sections 3 to 6 are, respectively, devoted to lasers with modulated losses, lasers with injected signals, lasers with feedback and bidirectional ring lasers. Section 7 discusses the « hyperchaos », or $1/f$ noise.

For a more complete approach to the problem, I refer to a recent monograph on the subject [9].

2. – Deterministic chaos.

2·1. *Historical aspects.* – Until recently the current point of view was that a few-body dynamics was fully predictable, and that only addition of noise sources, due to coupling with a thermal reservoir, could provide statistical fluctuations. Lack of long-time predictability, or turbulence, was considered as resulting from the interaction of a large number of degrees of freedom, as in a fluid above the critical Reynolds number (Landau-Hopf model of turbulence).

On the contrary it is now known that even in system with few degrees of freedom nonlinearities may give rise to expanding directions in phase space and this, together with the lack of precision in assigning initial conditions, is sufficient to induce a loss of predictability over long times.

This level of dynamical description was born with the three-body problem in celestial mechanics (Poincaré). Already a three-body dynamic system is very different from the two-body problem, since in general there are asymptotic instabilities. This means a divergence, exponential in time, of two phase-space trajectories stemming from nearby initial points. The uniqueness theorem for solutions of differential systems seems to offer an escape way: be more and more precise in localizing the co-ordinates of the initial point. However, a fundamental difficulty arises. Only rational numbers can be assigned by a finite number of digits. A « precise » assignment of a real number requires an infinite acquisition time and an infinite memory capacity to store it, and

neither of these two infinities is available to the physicist. Hence any initial condition implies a truncation. A whole range of initial conditions, even if small, is usually given and from within it trajectories may arise whose difference becomes sizable after a given time, if there is an exponential divergence. This means that predictions are in general limited in time and that motions are complex, starting already from the three-body case. In fact, we know nowadays from very elementary topological considerations that a three-dimensional phase space corresponding to three coupled degrees of freedom is already sufficient to yield a positive Liapunov exponent, and accordingly an expanding phase-space direction. This complexity is not due to coupling with a noise source as a thermal reservoir, but to sensitive dependence on initial conditions. It is called deterministic chaos.

The birth of this new dynamics was motivated by practical problems, as fixing the orbit of a satellite or forecasting meteorology [10], and it was strongly helped by the introduction of powerful computers. The mathematics of multiple bifurcations leading from a simple behaviour to a complex one is under current investigation. Some regularities, such as the « scenarios » or routes to deterministic chaos, have already been partly explored [11].

2·2. *Dynamical aspects.* – A dissipative system (*i.e.* with damping terms) does not conserve the phase-space volume. If we start with initial conditions confined in a hypersphere of radius ε, that is, with an initial phase volume

$$V_0 = \varepsilon^N ,$$

as time goes on, the sphere transforms into an ellipsoid with each axis modified by a time-dependent factor. Its volume is

$$V_t = \varepsilon^N \exp\left[\sum \lambda_i t\right]$$

(λ_i = Liapunov exponents). Since the volume has to contract, $V_t < V_0$, then

$$\sum_{i=1}^{N} \lambda_i < 0 .$$

We denote the sequence of λ exponents, starting from the smallest up to the highest, as the Liapunov spectrum. Let us consider for simplicity just the signs of nonzero λ_i, keeping the zero for $\lambda_i = 0$. We then describe a sequence of negative, zero and positive λ_i as, *e.g.*, $(- - 0 +)$. For $N = 1$, we have $(-)$ and a segment $V_0 = \varepsilon$ of initial conditions shrinks to a single point for $t \to \infty$, that is, the attractor is a fixed point. For $N = 2$, the system goes either to a fixed point $(- -)$, or to a limit cycle $(- 0)$. Chaotic motion $((- +)$ with $\lambda_i < |\lambda_-|)$ is forbidden in two dimensions by the Poincaré-Bendixon theorem. For $N = 3$, besides fixed point $(- - -)$ and limit cycle $(- - 0)$, we can have

motion on a torus with two uncommensurate frequencies $(- 0 0)$, but we can also have $(- - +)$, that is, a positive λ which gives an expanding direction along which we rapidly get uncertainty.

An example of chaotic motion is offered by the Lorenz model of hydrodynamic instabilities [10] which corresponds to the following equations where the parameter values have been chosen in order to yield one positive Liapunov exponent:

$$(1) \qquad \begin{cases} \dot{x} = -10x + 10y , \\ \dot{y} = -y + 28x - xz , \\ \dot{z} = -(8/3)z + xy . \end{cases}$$

The above considerations suggest to study low-dimensional chaos, with the simplest phase-space topology allowing for the appearance of a positive Liapunov exponent.

Focusing on these situations in quantum optics permits close comparison between experiments and theory. On purpose I do not tackle the vast class of inhomogeneously broadened lasers, where it is extremely difficult to derive close correspondences between experiments and theory because of the large number of coupled degrees of freedom.

If we couple Maxwell equations with Schrödinger equations for N atoms confined in a cavity, and expand the field in cavity modes, keeping only the first mode E which goes unstable, this is coupled with the collective variables P and Δ describing the atomic polarization and population inversion as follows:

$$(2) \qquad \begin{cases} \dot{E} = -kE + gP , \\ \dot{P} = -\gamma_\perp P + gE\Delta , \\ \dot{\Delta} = -\gamma_\parallel(\Delta - \Delta_0) - 4gPE . \end{cases}$$

For simplicity we consider the cavity frequency at resonance with the atomic resonance, so that we can take E and P as real variables and we have three coupled equations. Here, k, $\gamma_\perp$, $\gamma_\parallel$ are the loss rates for field, polarization and population, respectively, g is a coupling constant and Δ_0 is the population inversion which would be established by the pump mechanism in the atomic medium, in the absence of coupling. While the first equation comes from Maxwell equations, the two others imply the reduction of each atom to a two-level atom resonantly coupled with the field, that is, a description of each atom in a isospin space of spin $\frac{1}{2}$. The last two equations are like Bloch equations which describe the spin precession in the presence of a magnetic field. For such a reason eqs. (2) are called Maxwell-Bloch equations.

The presence of loss rates means that the three relevant degrees of freedom are in contact with a « sea » of other degrees of freedom. In principle, eqs. (2)

could be deduced from microscopic equations by statistical reduction techniques [5].

The similarity of Maxwell-Bloch equations (2) with Lorenz equations (1) would suggest the easy appearance of chaotic instabilities in single-mode, homogeneous-line lasers. However, time scale considerations rule out the full dynamics for most of the available lasers. Equations (1) have damping rates within one order of magnitude. On the contrary, in most lasers the three damping rates are wildly different from one another.

The following classification has been introduced [12]:

Class A (*e.g.*, He-Ne, Ar, Kr, dye): $\gamma_\perp \simeq \gamma_\parallel \gg k$.

The two last equations (2) can be solved at equilibrium (adiabatic elimination procedure) and one single nonlinear field equation describes the laser. $N = 1$ means fixed-point attractor, hence coherent emission.

Class B (*e.g.*, ruby, Nd, CO_2): $\gamma_\perp \gg k \geq \gamma_\parallel$.

Only polarization is adiabatically eliminated (middle equation (2)) and the dynamics is ruled by two rate equations for field and population. $N = 2$ allows also for period oscillations.

Class C (*e.g.*, FIR lasers): $\gamma_\parallel \approx \gamma_\perp \approx k$.

The complete set of eqs. (2) has to be used, hence Lorenz-like chaos is feasible.

We have carried a series of experiments on the birth of deterministic chaos in CO_2 lasers (class *B*). In order to increase by at least 1 the number of degrees of freedom, we have tested the following configurations:

i) Introduction of a time-dependent parameter to make the system nonautonomous [13]. Precisely, an electro-optical modulator modulates the cavity losses at a frequency near the proper oscillation frequency Ω provided by a linear stability analysis, which for a CO_2 laser happens to lie in the (50 ÷ ÷ 100) kHz range, making it easy an accurate set of measurements.

ii) Injection of signal from an external laser detuned with respect to the main one, choosing the frequency difference near the above-mentioned Ω. With respect to the external reference the laser field has two quadrature components which represent two dynamical variables. Hence we reach $N = 3$ and observe chaos [12].

iii) Use a bidirectional ring, rather than a Fabry-Perot cavity [14]. In the latter case the boundary conditions constrain the forward and the backward wave, by phase relations on the mirror, to act as a single standing wave. In the former case forward and backward waves have just to fill the total ring length with an integer number of wavelengths, but there are no mutual phase constraints, hence they act as two separate variables. Furthermore, when the field frequency is detuned with respect to the centre of the gain line, a complex population grating arises from interference of the two countergoing waves,

and as a result the dynamics becomes rather complex, requiring $N > 3$ dimensions.

iv) Add an overall feedback, besides that provided by the cavity mirrors, by modulating the losses with a signal provided by the output intensity [15]. If the feedback has a time constant comparable with the population decay time, it provides a third equation sufficient to yield chaos.

Notice that, while methods i), ii) and iv) require an external device, iii) provides intrinsic chaos. In any case, since feedback, injection or modulation are currently used in laser applications, the evidence of chaotic regions puts a caution on the optimistic trust in the laser coherence.

Of course, the requirement of three coupled nonlinear equations does not necessarily restrict the attention to just Lorenz equations. In fact, none of the explored cases i) to iv) corresponds to Lorenz chaos.

2·3. *Information aspects.* – Here, we discuss what we measure to assess chaos. We plot two of the 3 (or more) variables on a plane phase-space projection. This way, we build projections of phase-space trajectories on a x-y oscilloscope. Simultaneously we can measure the power spectrum. In sect. **3** we show a sequence of subharmonic bifurcations which eventually leads to an intricated trajectory (strange attractor) and to a continuous power spectrum. But how can we discriminate between deterministic chaos and noise? After all, noise also would give a continuous spectrum, and the phase-space point would fill ergodically part of the plane, thus covering a two-dimensional set.

In order to discriminate deterministic chaos from order as well as from random noise, we introduce two invariants of the motion, one static, the other dynamic.

We partition the phase space into small boxes of linear size ε and give i-th box a probability $p_i = M_i/M$ equal to the fractional number of times it has been visited by the trajectory. This way, we build a Shannon information $I(\varepsilon)$, and with it an «information dimension» $D_1(\varepsilon)$ [16] which is in general a fractional number, or a «fractal»:

$$I(\varepsilon) = -\sum_i p_i \log p_i , \tag{3}$$

$$D_1(\varepsilon) = \lim_{\varepsilon \to 0} \frac{I(\varepsilon)}{\log \varepsilon} . \tag{4}$$

To understand the meaning of a fractal, look after an operational definition of dimension [17]. Let us compare three sets: i) a segment of unit length; ii) the Cantor set, built by taking out the middle one-third of the unit segment and repeating the operation on each fragment; iii) the Koch curve, built by replacing the middle third with the other two sides of an equilateral triangle and repeating the operation *ad infinitum*. At each stage of the partition, we

cover each set with beads of suitable size not to lose in resolution (*e.g.*, diameter $\frac{1}{3}$ a the first partition) and count the number N for each set (at the first partition, we need 2 for the Cantor set, 3 for the segment, 4 for the Koch curve). We define the fractal dimension as the ratio

$$D_0(\varepsilon) = \frac{\log N(\varepsilon)}{\log (1/\varepsilon)}. \tag{5}$$

This definition is independent of the partition. Indeed for the Cantor set and the Koch curve we have $N = 2$, $\varepsilon = \frac{1}{3}$ and $N = 4$, $\varepsilon = \frac{1}{3}$, respectively, at the first partition, yielding

$$D_0(\text{Cantor}) = \frac{\log 2}{\log 3} \simeq 0.63 \ldots$$

and

$$D(\text{Koch}) = \frac{\log 4}{\log 3} \simeq 1.2618 \ldots .$$

At the second partition the number of necessary beads goes as N^2 and the diameter of each as ε^2, hence D_0 remains invariant.

Going back to the information dimension $D_1(\varepsilon)$, we see that we have replaced $\log N$ with $I(\varepsilon)$ which is an *average* (for p_i all equal, we recover $I(\varepsilon) = \log N$). Hence D_1 generalizes D_0 whenever the density of points is not uniform along the trajectory.

As D_0 was independent of the partition stage, similarly D_1 is an invariant, but static (time does not enter). It can be shown that $D_0 > D_1$, however for nonpathological sets the difference is irrelevant. Let us refer for simplicity to a $N = 3$-dimensional phase space. If $D = 0$ (fixed point) or 1 (limit cycle) or 2 (torus) we have an ordered, or coherent, motion. In the other limit of random noise, fluctuations fill ergodically a N-dimensional region of the space, hence $D = 3$. Deterministic chaos has to be in between, that is,

$$2 < D < 3 .$$

Hence a fractal dimension is an indicator of chaos. As we show later, this indicator is expressed in term of correlation functions, thus it requires the same measuring techniques introduced in photon statistics.

These features related to the topology of the attractor have a temporal counterpart in another invariant, which measures how information is dissipated in a motion to maintain knowledge on the system. To build this dynamic invariant, we partition both space and time in boxes of sizes ε and τ that we name $i_1, i_2, \ldots, i_d$ at each of the discrete times $\tau, 2\tau, \ldots, d\tau$, and introduce the joint probability over the d time intervals,

$$p_{i_1 i_2 \ldots i_d} \equiv \{x(t = \tau) \subset i_1; \ldots; x(t = d\tau) \subset i_d\} .$$

Correspondingly, we define a joint information

$$I_d(\varepsilon) = -\sum_{(i_1 \ldots i_d)} p_{i_1 \ldots i_d} \log p_{i_1 \ldots i_d} . \tag{6}$$

Then, by a limit operation, define the Kolmogorov entropy as the rate of information loss per unit time:

$$K \equiv \lim_{\tau \to 0} \lim_{\varepsilon \to 0} \lim_{d \to \infty} \frac{1}{d\tau} \sum_{n=1}^{d} (I_{n+1} - I_n) = \lim \frac{1}{d\tau} I_d . \tag{7}$$

Now we have two indicators to gauge the difference among *order*, *random noise* (Brownian motion) and *deterministic chaos*. Referring to K, it is easily seen that

$K = 0$ for order (no information loss),

$K = \infty$ for random noise (total information loss),

$0 < K < \infty$ for deterministic chaos.

The box counting method described above is impractical. It may require 10^6 points for a convergent numerical result. On the contrary, the following method introduced by GRASSBERGER and PROCACCIA [18] is applicable to only $10^3 \div 10^4$ independent data points. We generalize Shannon information defining the order-f information as

$$I_f(\varepsilon) = \frac{1}{1-f} \ln \sum_i p_i^f . \tag{8}$$

For $f \to 1$ we recover the usual definition. Associated with I_f, there is an order-f dimension of the attractor

$$D_f = \lim_{\varepsilon \to 0} \frac{I_f(\varepsilon)}{\ln (1/\varepsilon)} . \tag{9}$$

For $f = 0$ and 1 we recover D_0 and D_1. Consider $f = 2$. The sum $\sum p_i^2$ is just the probability that a pair of random points on the attractor fall into the same box, that is, that two arbitrary points will have a distance less than ε. Calling this probability $C(\varepsilon)$, we expect thus

$$C(\varepsilon) = \lim_{N \to \infty} \frac{1}{N^2} \sum_{ij} \theta(\varepsilon - |x_i - x_j|) \simeq \varepsilon^{D_2} , \tag{10}$$

where $C(\varepsilon)$ is measured as the number of pairs (i, j) with a distance $|x_i - x_j| < \varepsilon$. Here θ is the Heaviside step function.

Experimentally, we do not measure at each time the vector $x(t)$ of phase space, but just one component $x_i(t)$ (for instance, just the light out of a laser). However, in a nonlinear system, any component $x_k(t)$ will influence x_i at a later time (no normal-mode transformation!). Hence, we can build a m-dimensional phase space $\xi(t)$ by just measuring one single component x_i at successive times and considering the m-fold as a single point in m-space:

$$\xi(t) \equiv [x_i(t), x_i(t+\tau), \ldots, x_i(t+m\tau)]\,. \tag{11}$$

As we evaluate the slope $\log C$ *vs.* $\log \varepsilon$ from our data, we can stop from increasing m when the slope shows saturation. The saturated slope is D_2.

3. – The modulated laser [13, 19].

For a single-mode, class-B, laser tuned at the centre line, the phase space becomes two-dimensional, however introduction of a time-dependent parameter makes the system nonautonomous adding a third equation and thus making it possible the appearance of a positive Liapunov exponent. It is then a practical matter to localize the values of the control parameters (pump, modulation frequency and amplitude) for which this will occur.

When we apply a time-dependent loss, the laser equations become

$$\begin{cases} \dot{I} = 2kI(z-1)\,, \\ \dot{z} = -\gamma_\perp(z_0 - z - zI)\,, \\ \dot{k} = mk_1\Omega\sin\Omega t\,. \end{cases} \tag{12}$$

They come from (2), eliminating P and rescaling $I = F^2$ and $z = \Delta$. For $m \to 0$, we have small deviations from the equilibrium values

$$\begin{cases} \bar{I} = z_0 - 1\,, \\ \bar{z} = 1\,. \end{cases} \tag{13}$$

These deviations are linear in m and synchronous with the external frequency Ω. Destabilization of this limit cycle has to be dealt with by Floquet theory [20]. It may be shown that even for $m \to 0$ a nonlinear resonance yields a positive Liapunov exponent for Ω around the characteristic frequency [13]

$$\Omega \simeq \sqrt{2k_1\gamma_\perp(z_0-1)}\,. \tag{14}$$

For a CO_2 laboratory laser near threshold $k \simeq 3\cdot10^7\ s^{-1}$, $\gamma_\perp \simeq 10^4\ s^{-1}$ and $z_0 - 1 \simeq 0.1$ (10% above threshold), the corresponding frequency $f = \Omega/2\pi$ is in the 50 kHz range, easily accessible.

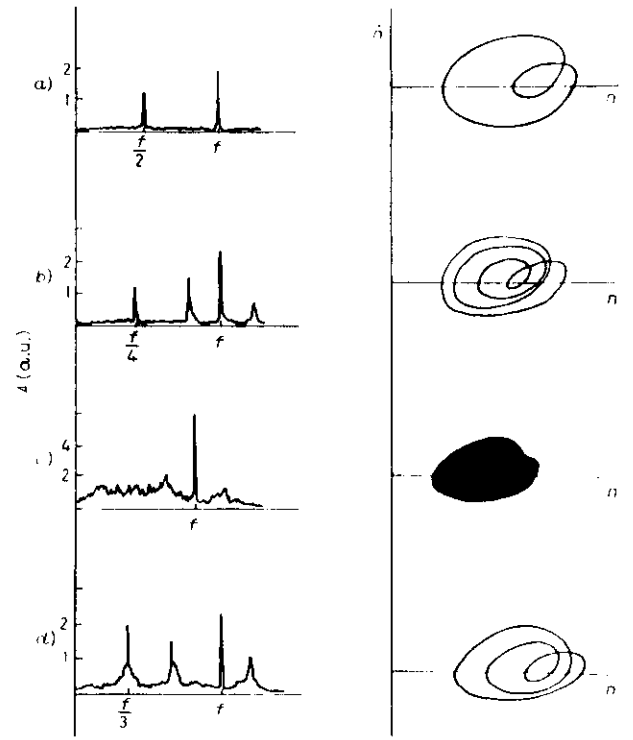

Fig. 1. – Experimental phase-space portraits ($n - \dot{n}$) (right-hand side) and the corresponding frequency spectra (left-hand side) for different modulation frequencies f: *a*) f = 62.7 kHz. Period-two limit cycle and corresponding $f/2$ subharmonic. *b*) f = 63.80 kHz. Period-four limit cycle and $f/4$ subharmonic. *c*) f = 64.00 kHz. The phase-space portrait shows a strange attractor (the oscilloscope spot could not resolve single windings). The power spectrum is a quasi-continuous one with a small peak at the modulation frequency (see the scale change with respect to previous figures). *d*) f = 64.13 kHz. Period-three limit cycle and $f/3$ subharmonic.

Thus we have made two series of experimental observations, the first [13] devoted to an experimental assessment of chaotic instabilities by phase-space portraits and power spectra, the second [19] to fractal dimensions and Kolmogorov entropy.

The driving frequency f was chosen to vary in the region from $\Omega/2\pi$ to its third harmonic, that is from 60 to 190 kHz. We have explored modulation values between 1% and 5%. A complete state diagram would yield the dynamical features for all possible values of the modulation parameters m and Ω. However, the strip m = 1% - 5% does not display m dependence; therefore, we limit ourselves to giving experimental results at m = 1% for various Ω values.

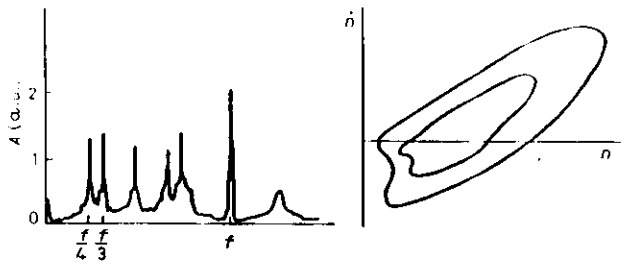

Fig. 2. – f = 63.85 kHz. Experimental evidence of generalized multistability (coexistence of two independent attractors). The power spectrum shows that those attractors correspond to $f/3$ and $f/4$ subharmonic bifurcations, respectively; in phase space, the multiple windings merged within the thickness of the phase portrait contour.

The experimental set-up consists of a CO_2 laser carefully stabilized against thermal and acoustic disturbances, with the discharge current stabilized better than $1/10^3$. No long-term stabilization was necessary. The electro-optical modulator was a CdTe, antireflex-coated, 6 cm long crystal, with an absorption loss than 0.2 %. The laser cavity includes also a $\lambda/4$ plate and a beam expander, both coated to limit the total losses per pass to 20 %. The laser output is detected on a fast (2.5 ns rise time) pyroelectric detector whose current, proportional to the photon number $n(t)$, is sent together with its time derivative $\dot{n}(t)$ to a x-y scope, in order to have the phase-space portrait $(n, \dot{n})$. The detector is also sent to a Rockland spectrum analyser to measure the power spectra.

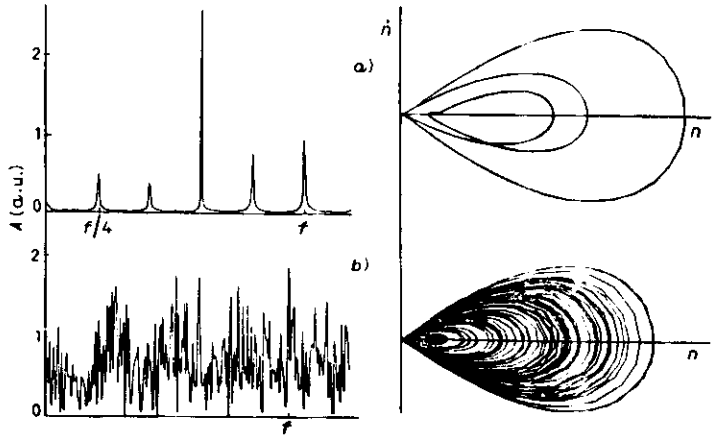

Fig. 3. – Computer plots for the parameter values $\gamma_1 = 10^3\ s^{-1}$, $K = 7 \cdot 10^7\ s^{-1}$, $m = 2.0 \cdot 10^{-2}$, $GE = 2.0 \cdot 10^{11}$. *a*) f = 64.33 kHz. Subharmonic bifurcation $f/4$, as in the experiment of fig. 6*b*). *b*) f = 78.8 kHz, m = $3 \cdot 10^{-2}$. Strange attractor and broad spectrum corresponding to a chaotic solution.

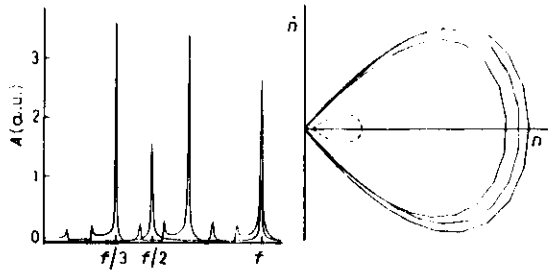

Fig. 4. – Theoretical generalized bistability; f = 119.0 kHz, m = $2.0 \cdot 10^{-2}$. The phase-space portrait shows the existence of two independent attractors, corresponding to the subharmonic frequencies $f/2$ (dashed line) and $f/3$ (continuous line); relative spectra are superimposed. It must be noted that one attractor remains inside the other as in the experiment of fig. 2. If initial conditions are properly changed, a third attractor is found with a superharmonic frequency $f/10$ (not plotted for the sake of simplicity). Initial conditions: $n_0 = 4 \cdot 10^6$, $\dot{n} = 0$ (dashed), $n_0 = 2 \cdot 10^5$, $\dot{n}_0$ = $2 \cdot 10^6$ (continuous).

The limited range (up to 100 kHz) of the spectrum analyser has limited the frequency range explored in this first run. We show later that interesting bifurcations are also expected in the 180 kHz domain.

In fig. 1 we show experimental data in a narrow region between 62.7 and 64.13 kHz where various bifurcations occur. This region is limited above and below by wide intervals with stable single-period limit cycles. Figure 1*a*) shows the $f/2$ bifurcation at f = 62.7 kHz, fig. 1*b*) the $f/4$ case for f = 63.8 kHz, fig. 1*c*) shows the strange attractor and a broad-band spectrum for f = 64.0 kHz, and fig. 1*d*) shows the $f/3$ case for f = 64.13 kHz.

Furthermore, at f = 63.85 kHz a new feature appears, namely the coexistence of two independent stable attractors, one of period $4(f/4)$ and the other of period $3(f/3)$ (fig. 2). This bistable situation has nothing to do with the common optical bistability where two d.c. output amplitude values appear for a single d.c. driving amplitude. We call this coexistence of two attractors « generalized bistability » (see sect. 7).

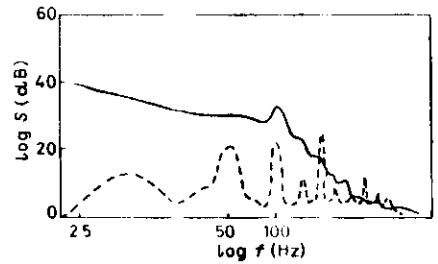

Fig. 5. – Experimental power spectra in the case of two attractors, stable (dashed line) and strange (solid line).

In fig. 3 and 4 we report the theoretical equivalents of fig. 1 and 2, respectively, obtained by computer solution of eqs. (12) with parameter values in the range of the experiment.

As stated in sect. 7, $1/f$-type low-frequency divergences, with power spectra as $f^{-\alpha}$ ($\alpha = 0.6 \div 1.2$), appear when the following conditions are fulfilled: i) There are at least two basins of attraction, ii) the attractors have become strange and any random noise (always present in a macroscopic system) acts as a bridge, triggering jumps between them. These jumps have the $f^{-\alpha}$ feature. In the region of bistability (see fig. 2) we have increased the modulator amplitude m up to the point where the two attractors have become strange. Figure 5 shows the sudden increase in the low-frequency spectrum. The divergent part has a power law behaviour $f^{-\alpha}$ with $\alpha \simeq 0.6$.

The above-described first run is still affected by the experimental uncertainties which characterize a phase-space projection or a power spectrum. Does the first one show a self-similar structure beyond the chaotic threshold as theoretically expected for a strange attractor, or it just fills ergodically a two-dimensional region of the $(n, \dot{n})$ plane, thus being trivial random noise? After all the latter test (continuous frequency spectrum) is also a common property of random noise and it is not a sufficient characterization of deterministic chaos.

In order to set a more reliable distinction between chaos and random noise, and also to specify the route to chaos (fig. 1 is only a preliminary evidence of a Feigenbaum, on subharmonic, route), we have digitized the signal by a LeCroy transient recorder with 32000 samples in memory. Setting the internal clock at 320 ns, we obtained approximately 16 points for each period of the fundamental frequency with light-bit resolution. By synchronizing the sampling time to the external drive period we obtained a projection of the Poincaré section. The projection is onto a one-dimensional space (we measure only the intensity) independent of the other variables. In fig. 6 we present the sections and the corresponding time series, respectively. The advantage of this signal processing is that we are able to analyse a high number of periods (32000 maximum) with a single acquisition. Furthermore, it allows a much larger-bandwidth processing of narrow pulse sequences, which otherwise requires a high sampling rate with the related problems in data storing and processing. In fig. 6, on the left-hand side, the bandwidth is 300 kHz, and on the right it is 100 MHz; indeed we can notice already in the $f/8$ plot a loss of resolution in the smaller peaks on the left-hand side.

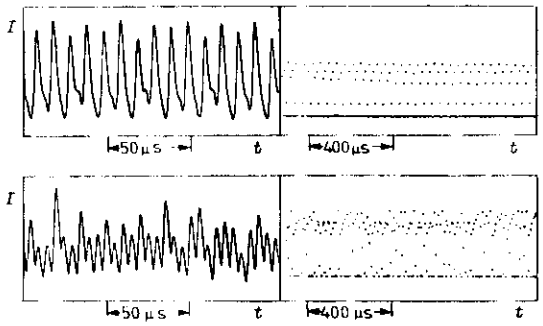

Fig. 6. – Top: Laser intensity *vs.* time for a $f/8$ subharmonic frequency, and corresponding stroboscopic intensity plot with the time interval between successive points equal to the period of the modulation frequency (191.000 kHz). Bottom: Laser intensity *vs.* time and stroboscopic plot for chaotic behaviour. The period of the modulation is 5.2 μs. We note on the left-hand side the loss of resolution due to the limited acquisition bandwidth. This drawback is absent on the right-hand side because of the huge increase in bandwidth.

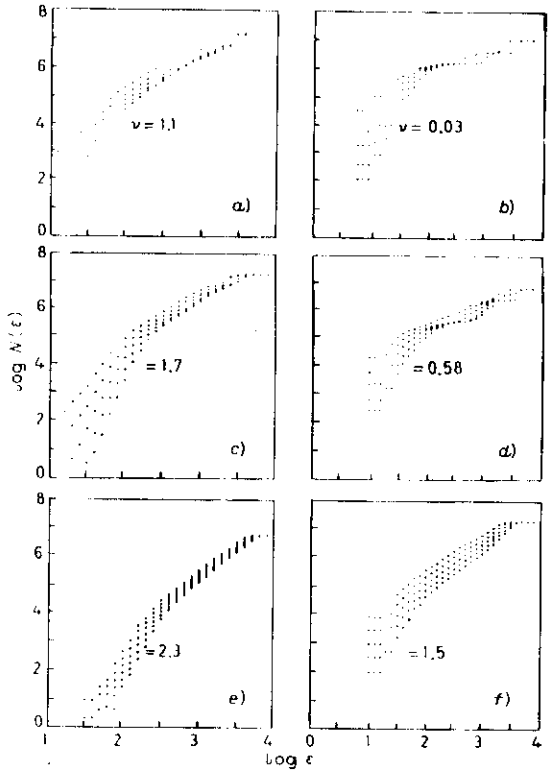

Fig. 7. – Plots of $\log N_n(\varepsilon)$ *vs.* $\log \varepsilon$ for different values of n calculated from the time series (left-hand panels) and from the stroboscopic sections (right-hand panels) for different subharmonic frequencies: *a*), *b*) $f/4$; *c*), *d*) $f/8$; and *e*), *f*) chaotic behaviour. All best-fit values of the slope ν are assumed to have an overall estimated error of ± 0.1. 6000 points were used. The embedding dimensions for all reported plots run from 5 to 9. Dimensions from 1 to 15 were tested.

We analyse digitized time sequences of the laser output intensity and reconstruct the attractors with an embedding technique. For the determination of the fractal dimension we follow the method of Grassberger-Procaccia.

If we define $N_n(\varepsilon)$ as the number of vectors whose distance is smaller than ε, and if the embedding dimension n is large enough, then $N_n(\varepsilon) \sim \varepsilon^\nu$, where ν is the D_2 dimension of the attractor. In fig. 7*a*) to *f*) we plot $\log N_n(\varepsilon)$ as a function of $\log \varepsilon$ for a sequence of bifurcations *f*/4, *f*/8, and chaos. We limit our analysis to the regions where the slope remains constant over a wide region of $\log \varepsilon$ and where it is independent of n, as it must be from theoretical predictions.

From inspection of fig. 7*a*) and *b*) it is clear that the slope obtained for the *f*/4 subharmonic saturates at $\nu \sim 1$ in the time series and $\nu \sim 0$ in the Poincaré section. For the *f*/8 subharmonic ν is slightly above 1.5 (fig. 7*c*) and *d*)). This result, even though not readily understandable because the time signal still appears periodic, nevertheless agrees with the theoretical prediction for the dimension at the accumulation point (infinite periodicity) of the logistic map ($1.537\,6 < \nu < 1.533\,85$). Indeed this dimension has been proven to be universal for those mappings for which the Feigenbaum scaling law holds [21]. We present here a heuristic interpretation based on our data. In our experimental system, the unavoidable noise yields a trajectory wandering over a nonzero range of parameter values, the «testing» nearby periodic attractors of the subharmonic sequence. For infinite resolution, we would see for the stroboscopic data a staircase of horizontal plateaus each with zero slope, as it appears at higher embedding dimensions in fig. 7*b*) and *d*). However, the finite resolution of the correlation measurements averages over adjacent steps, and thus provides the 0.58 slope, as it appears in fig. 7*d*). This is the first time that the dimension at the accumulation point of a Feigenbaum cascade has been measured in an experimental system.

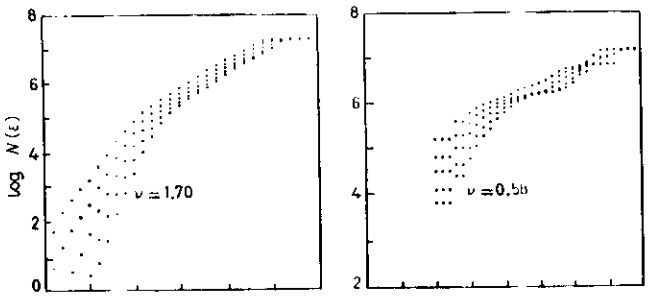

Fig. 8. – Plots of $\log N(\varepsilon)$ *vs.* $\log \varepsilon$ for different dimensions n obtained from the numerical integration of the model equations for two different cases, *f*/8 subharmonic (left-hand side) and chaos (right-hand side). 6000 points were used.

When the system enters the chaotic region, the fractal dimension suddenly jumps to a higher value ($\nu = 2.4$).

The time behaviour of the intensity obtained by numerical integration of eqs. (12) was processed in the same manner as the experimental signal. Figure 8 shows the results obtained for a *f*/8 solution and a strange attractor. Again near the accumulation point $\nu \sim 1.5$. Direct comparison of fig. 8 with fig. 7*c*) and *d*) shows good agreement between experiment and model.

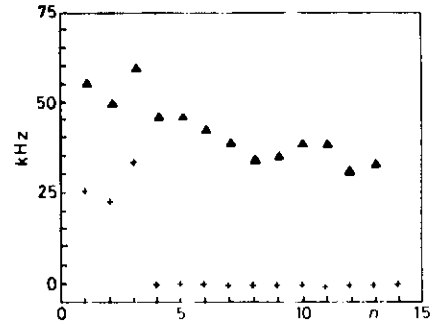

Fig. 9. Correlation entropy K_2 (in kilohertz) *vs.* the embedding dimension for the *f*/4 (crosses) and the chaotic (triangles) attractor.

In fig. 9 we report the correlation entropy K_2 *vs.* the embedding dimension for the *f*/4 and for the chaotic attractor, *vs.* the embedding dimension, from the data of fig. 7. We see that, while $K_2 = 0$ for *f*/4, $K_2 \simeq 35$ kHz for the chaotic attractor. As we have a single positive Liapunov exponent and as the embedding time is 5.2 μs, we estimate that the half-loss of information corresponds to 3.8 periods of the modulation frequency.

4. – The laser with injected signal (LIS) [12, 22, 23].

Injecting an external signal into a single-mode laser provides an extra degree of freedom. Indeed, in general, the field amplitude x has to be decomposed into two dynamical variables, that is, the two quadrature components $x_1 + ix_2 = x$ with respect to the external phase reference. In class *C* lasers this provides a fourth equation [24, 25] which is more than the necessary requirement for deterministic chaos. A simpler situation is that of a class *B* LIS, which is ruled by the three equations

$$(15)\qquad \begin{cases} \dot{I}/2k = Iz(1+\delta^2)^{-1} - I + \sqrt{I}x_0 \cos\varphi\,, \\ \dot{\varphi}/k = -\theta - \delta z(1+\delta^2)^{-1} - x_0 \sin\varphi/\sqrt{I}\,, \\ \dot{z}/\gamma_1 = z_0 - z - zI(1+\delta^2)^{-1}\,, \end{cases}$$

where $x_0 = A$ is the external field and $x = \sqrt{I}\exp[i\varphi]$ the internal one. The frequency relations among gain line, cavity, external field and internal laser are given in fig. 10.

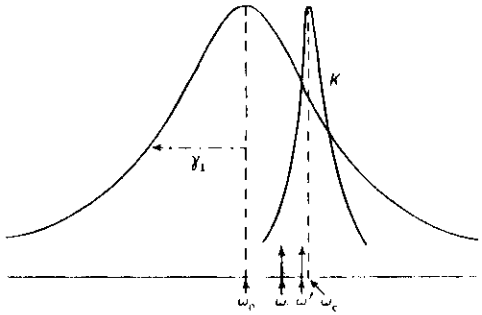

Fig. 10. – Qualitative plot of the frequency relations among atomic resonance (homogeneous width $\gamma_\perp$) centred at ω_0, cavity resonance (width K) centred at ω_c and injected field at ω_1.

We have observed two different ways to reach the locked regime, either by decreasing the oscillation frequency (tangent bifurcation), or by decreasing the amplitude of oscillation (Hopf bifurcation), and two different routes to chaos, either by intermittency or by period doubling.

An extensive linear stability analysis was reported in ref. [22], together with numerical solutions of eqs. (15) for different values of the injected amplitude $A = x_0$ and mutual detuning $\theta - \delta$.

Preliminary experimental data have been obtained by a three-laser set-up [23], the first laser being a ring laser where the dynamics develops, the second one the external injecting laser and the third one a master oscillator with reference to which first and second laser are stabilized. The parameter region explored in this experiment was sufficient to yield oscillatory instabilities but not enough to reach chaos.

5. – The laser with feedback [15].

In laser applications where high stability is required, an overall negative feedback is currently used, besides that already provided by the electromagnetic cavity, for instance by controlling the pump strength with a signal provided by the detected output intensity. However, a fundamental objection to a feedback scheme is that it provides one extra dimension to phase space and hence the modified dynamics can be affected by irregular behaviour.

Here we show how feeding the laser output back on an intracavity modulator introduces a third degree of freedom leading to chaotic instability. When the feedback loop is so fast that it practically provides an «instantaneously» adapted loss coefficient, it does not modify the phase-space topology, which in the case of a class B laser remains two-dimensional. If, however, the time scale of the feedback loop is of the same order as that of the other relevant variables, the system becomes three-dimensional. Such a system is ruled by three first-order equations for the intensity x, population difference z and modulation voltage v. With suitable normalizations (notice that here x is the intensity, *not* the field) the equations are

$$\text{(16)} \qquad \begin{cases} \dot{x} = -kx(1 + \alpha \sin^2 v - z), \\ \dot{z} = -\gamma_\parallel(z - A + xz), \\ \dot{v} = -\beta(v - B + fx), \end{cases}$$

where $k(v) = k_0(1 + \alpha \sin^2 v)$ is the loss rate modulated by the voltage v, k_0 is the nonmodulated cavity loss parameter, α the coupling between detector voltage v and modulator, $\gamma_\parallel$ the population decay rate and β the damping constant of the feedback loop. Furthermore, B is the voltage bias applied to the second input of the modulator amplifier, A is the pump parameter, f is a coupling coefficient between intensity x detected on D and voltage v. Notice that x is normalized to the saturation intensity, z and A to the threshold population (without feedback) and v is given in angular units.

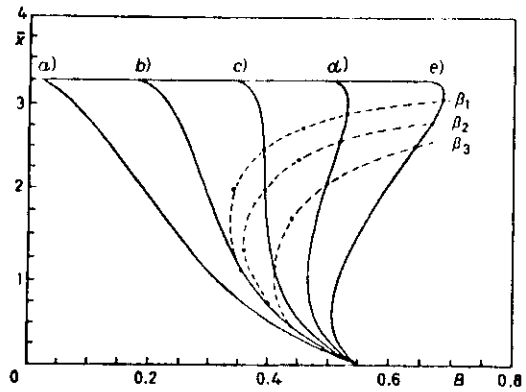

Fig. 11. – Laser with feedback: plots of normalized stationary intensity $\bar{x}$ *vs.* B (the bias voltage B is expressed in angular units) for different values of the feedback coupling constant f. The curves *a*) to *e*) refer to $f = 0$, 0.052, 0.102, 0.152 and 0.202, respectively. Dashed lines correspond to the loci of the first Hopf bifurcations for three different values of the damping constant (s^{-1}) of the feedback loop, namely, $\beta_1 = 3.5 \cdot 10^4$, $\beta_2 = 3.0 \cdot 10^4$ and $\beta_3 = 2.5 \cdot 10^4$.

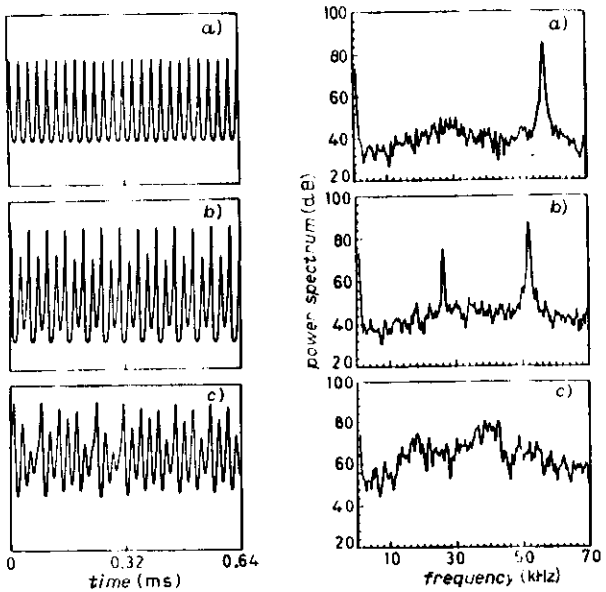

Fig. 12. – Laser with feedback: digitizer time plots of the experimental laser intensity (left) and the corresponding power spectra (right) for increasing values of the control parameter B. *a*) corresponds to the onset of the first Hopf bifurcation, at a frequency $\nu = 57.3$ kHz, $B = 0.364$; *b*) shows the appearance of a subharmonic bifurcation $f/2$ where the fundamental frequency is $\nu = 52.0$ kHz, $B = 0.378$ and *c*) shows the appearance of chaos, $B = 0.383$.

The experimental system of ref. [15] has $k_0 = 1.17 \cdot 10^7\ (s^{-1})$, $\gamma_\perp = 0.98 \cdot 10^4\ (s^{-1})$, $\beta = 3.0 \cdot 10^4\ (s^{-1})$ and a normalized pump $A = 4.2$.

The stationary solutions $(\bar{x}, \bar{y}, \bar{z})$ of eqs. (16) imply the condition

$$B = f\bar{x} + \arcsin\left(\frac{A/\alpha}{1 + \bar{x}} - \frac{1}{\alpha}\right). \tag{17}$$

Depending on the feedback coupling f, for different bias values B we can have mono or bistability (fig. 11). In particular, around $f = 0.1$ we expect an ambiguity, since eq. (17) provides a quasi-vertical curve. Indeed, as we show later, this is the region where we observe chaos.

By a linear stability analysis around the stationary solution, we evaluate the points where the system starts self-pulsing (Hopf bifurcations). The lines of Hopf bifurcations are drawn in fig. 11 (dashed) for three different β values.

In fig. 12 we present the power spectra of the intensity detected in the experiment. Figure 12*a*) shows the first Hopf bifurcation, fig. 12*b*) the appearance of a subharmonic $f/2$, and fig. 12*c*) corresponds to the appearance of chaos.

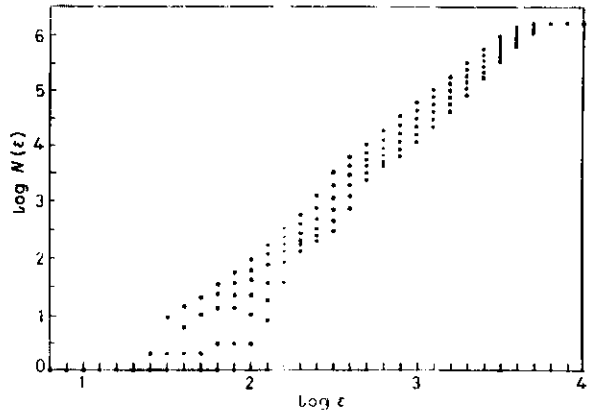

Fig. 13. – Laser with feedback: plots of $\log N_n(\varepsilon)$ *vs.* $\log \varepsilon$ for different values of embedding dimension n ($n = 10 \div 15$); $D_2 = 2.6 \pm 0.1$. Full dots come from experiment. Theoretical plots coincide with the experimental ones within the dot sizes.

Beyond chaos, there are periodic time windows. In order to get full assurance of the chaotic nature of the time plot of 12*c*), the correlation dimension was measured.

Figure 13 shows a fractal exponent $D_2 = 2.6 \pm 0.1$. While fig. 13 comes from the experiment, the same D_2 value is obtained by solving numerically eqs. (16) for $\beta = \beta_2 = 3.0 \cdot 10^4$ and $B = 0.383$. The theoretical plots, when reported in fig. 13, closely follow the experimental ones with uncertainties smaller than the dot sizes.

6. – The bidirectional ring laser [14].

Last we consider a longitudinal single-mode CO_2 ring laser in which both directions of propagation are allowed (fig. 14). The linewidth being homogeneously broadened, the two counterpropagating beams cannot work at the same time, because they must compete for the same amount of population inversion. Moreover, they are slightly detuned between each other—and with respect to line centre—because, for intrinsic asymmetries, cavity losses are different on the two propagation directions (K_1 and K_2); this results in a different mode pulling and then different lasing frequency. Indeed, having a gas flow in the laser tube, this already induces a small amount of Doppler shift in the interaction with one or the other of the two counterrunning modes. The detuning has been shown experimentally as well as in the numerical solution to be essential for breaking the symmetry between the two directions. A forbidden gap around the centre of the molecular line, as well as the inter-

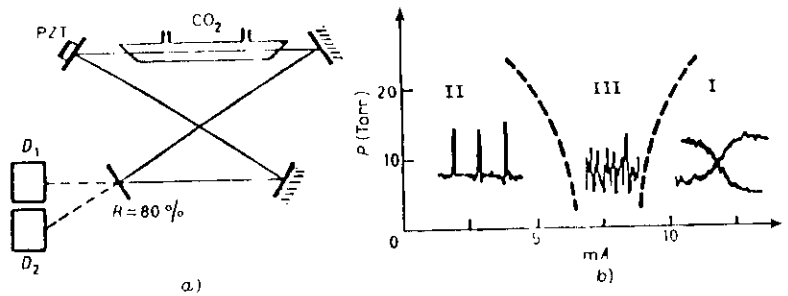

Fig. 14. – Bidirectional ring laser: *a*) Experimental set-up: gain cell with partial pressures: CO_2 1, N 1.5 Torr, He variable. Cavity length 4.2 m; PZT piezoelectric mirror translator; D_1 and D_2 detectors for forward and backward intensities. *b*) Phase diagram for total pressure (P) and discharge current (i). Regions are: I mode alteration, II self Q-switch, III irregular pulsation.

change of role of forward and backward fields at right and left of the line centre are evidence of such a detuning. If $K_{1,2}$ were the « cold » damping rates, they could not differ for reciprocity (in a passive medium thermodynamics forbids such a simmetry breaking). However, the $K_{1,2}$ in the active medium differ for the above-mentioned gas flow effect.

Through the grating induced in the population inversion by the interference of the two waves we have an interchange of energy from one field into the other by backscattering, so that we may consider the system as a LIS (where the injection comes from the counterpropagating mode).

In the experimental parameter space (fig. 14) we can distinguish three main different regions showing completely different behaviour. In the first one we observe a self-pulsing very similar to that of the laser with an injected signal.

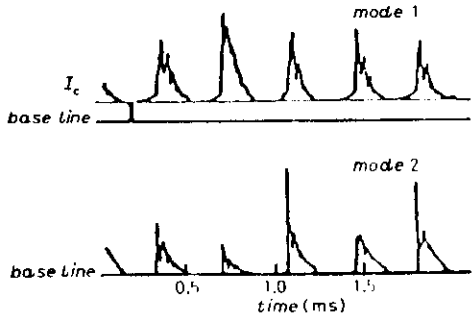

Fig. 15. – Bidirectional ring laser, region II: output intensity *vs.* time. The upper signal has a c.w. baseline, while the lower oscillates over a zero level. Oscillations relax to the steady state before a new jump (interchange between c.w. action) takes place.

One mode is also running c.w., while in the other one we observe only spikes, in phase with the main mode, which occur at a repetition rate (ω_s) of the order of $\gamma_\parallel$. In fact, as in the LIS system, the c.w. working mode injects some energy into the other one letting population inversion increase up to a level at which a giant pulse takes place (the height may be 500 times greater than the stationary level). During the pulse both modes go above threshold and spike in phase. Superimposed to the decay we see relaxation oscillations typical of CO_2 lasers with a frequency (ω_0) very near to Ω: they are out of phase because of competition between the two modes.

For higher excitation currents we observe a deterministic switching due to competition between the two fields with low frequency (30 Hz). During interchange jumps we observe again the two frequencies of fig. 15 but with the lower one increased because of a larger value of $\gamma_\parallel$ (higher current), while the higher one can be varied also by adjusting the cavity length and alignment by moving a mirror mounted on a piezoelectric crystal.

The transition between these two regimes is not abrupt and it takes place through a region which shows chaotic behaviour. Here both phenomena related to population inversion, spiking (lower currents) and oscillation (higher currents), take place; effective output frequency results also as a combination of the two others ($\omega_s \pm \omega_0$). At the same time, if we adjust the cavity mirror position so that we bring $\Omega \simeq \omega_s \pm \omega_0$, we obtain a competition of two different variables (population inversion and field) on the same time scale. The result is a fully developed chaos (fig. 16).

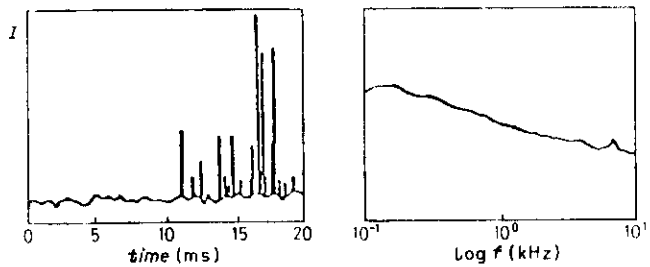

Fig. 16. – Bidirectional ring laser, region III: output intensity *vs.* time for a wholly chaotic signal (left). Double logarithmic power spectrum with low-frequency divergence $f^{-\alpha}$, $\alpha \sim 0.6$ (right).

If now we inject back one field into the laser with an external mirror (a fifth mirror in the configuration of fig. 14) we obtain stabilization of self-spiking, stable laser action instead of switching between the two modes and chaotic behaviour. At the boundary between the spiking and the chaotic region we observe a phenomenology typical of a laser with an injected signal (fig. 17).

It means that in this situation we have parameters practically equal to those responsible of such a behaviour in the LIS case, although the system here is more complicated.

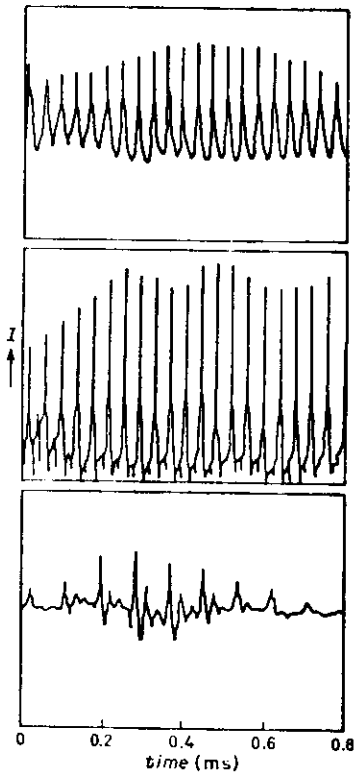

Fig. 17. – Bidirectional ring with extra mirror to reinject the forward mode into the backward one: output intensity *vs.* time. Bifurcation sequence in analogy with a laser with injected signal.

7. – Noise-induced trapping at the boundary between two attractors: hyperchaos and 1/*f* spectra [26].

In this section we show how addition of random noise in a nonlinear dynamical system with more than one attractor may lead to 1/*f* spectra, provided that the basin boundary be fractal. This shows that combining the features leading to deterministic chaos with a random noise is somewhat equivalent to a double randomness and we call « hyperchaos » such a situation. Indeed random-random walks in ordinary space, as diffusion in disordered systems,

have shown a 1/*f* behaviour [27, 28]. Thus hyperchaos here introduced is a random-random walk in phase space, where in fact one of the two sources of complex behaviour is due to the fractal structure arising from deterministic dynamics.

To evaluate the impact of the following arguments, we premise some historical remarks on 1/*f* spectra in nonlinear dynamics.

Some years ago it was discovered [29] that, in a nonlinear dynamical system with more than one attractor, introduction of random noise induces a hopping between different basins of attraction, giving rise to a low-frequency spectral divergence, resembling the 1/*f* noise well known in many areas of physics [30]. Such a discovery was confirmed by a laser experiment implying two coexisting attractors [13] already reported in sect. 3, and later the effect was observed in other areas as, *e.g.*, Josephson tunnel junctions [31, 32].

The effect was questioned with two objections:

a) a noise-induced jump across a boundary leads to a telegraph signal, hence to a single Lorentzian spectrum [33*a*];

b) a computer experiment yielded a power law only over a limited spectral range [33*b*].

The questions were answered [33*c*] with a statement of the empirical conditions under which the 1/*f* spectra appeared, namely:

i) coexistence of at least two attractors (so-called « generalized multistability » [13]),

ii) presence of noise,

iii) some « strangeness » in the attractors.

As a matter of fact this third condition was rather vague. To make it more precise, two theoretical models were explored, namely, a one-dimensional cubic iteration map with noise [34] and a forced Duffing equation with noise [35]. Both these papers disclose interesting features, bringing more light on the above assumption iii). Figure 2 of ref. [34] shows that the size of the 1/*f* spectral region increases with the r.m.s. of the applied noise, that is, with the probability of crossing the basin boundary by a noise-induced jump (fig. 3 of the same reference shows that the Liapunov exponent approaches the crisis value for increasing noise).

The numerical evaluation of ref. [35] showed that for some control parameters the boundary between basins of attraction was an intricated set of points, through which it was impossible to draw a simple line. In such cases the noise was most effective in yielding low-frequency spectra 1/*f*-like.

On the other hand, a fundamental logical approach to the 1/*f* problem was based on the composition of a large number of Lorentzians (or elementary Markov processes with exponential decay) whose weights are log-normally

distributed [36], thus fulfilling the relation

$$\int_{\gamma_1}^{\gamma_2} \frac{\gamma}{\omega^2 + \gamma^2} p(\gamma)\, \mathrm{d}\gamma \simeq \mathrm{const} \cdot \frac{1}{\omega}, \tag{18}$$

provided $p(\gamma) \sim 1/\gamma$, and for the frequency range $\gamma_1 \ll \omega \ll \gamma_2$.

Motivated by the rate processes considerations of ref. [33*a*], which yielded a single Lorentzian for two attractors, we developed a kinetic model [34] based on a single transition rate for each pair of attractors. In the case of M attractors, this yielded $M - 1$ Lorentzians. To approximate the integral (18) by a sum (5 % accuracy in fitting a $1/f$ law would require about one pole per decade) a large number $M \gg 2$ of attractors is necessary and hence the integral of eq. (18) would be replaced by the sum over the $M - 1$ Lorentzians corresponding to the eigenvalues of the kinetic model, however there is no reason to weigh the Lorentzians according to their reciprocal widths, hence no satisfactory reconstruction of a $1/f$ spectrum was possible. In fact, an experiment on a forced and noisy Duffing oscillator with an increasing number of attractors [37] did not offer clear evidence of the expected scaling of the spectral exponent with the number of attractors. On the contrary, ref. [35] showed that the boundary region between just two attractors was sufficient to yield $1/f$-like spectra, at variance with the many-attractor model. Thus this suggested that the boundary structure was the real responsible for a large number of decay constants (possibly log-normally distributed).

In the meantime, the fractal structure of a basin boundary was explored in some examples [38]. This means the following. As the phase point wanders within one basin of attraction, if we draw a sphere around the point defining its distance from the other basin of attraction, the radii of these spheres are distributed with all scale lengths, according to the self-similar structure of the fractal boundary. If we consider two-dimensional projections of the phase space as in fig. 3 to 6 of ref. [35], the spheres will be circles.

Based on the above considerations, we have built an elementary cellular automaton which models the motion of the phase point within a fractal basin boundary under the presence of random noise. We model the boundary region of two basins of attraction A and B as two adjacent one-dimensional lattices of sites. Suppose we start from site i. At each discrete time step, if i belongs to A ($i = i_A$) it moves one step forward on the same lattice ($i_A \to i_A + 1$) and if it belongs to B it goes one step backward ($i_B \to i_B - 1$). In the absence of noise, once the motion has started on one basin, it will remain on it forever. In the presence of noise, at each time step there is a finite probability of a « cross » jump at the same lattice site, from strip A to B: $i_A \to i_B$.

We call L the maximum size of the boundary region and $l_i \leq L$ any of the possible sizes of the fractal set. At each time step, the probabilities of permanence and jump are, respectively,

$$\begin{cases} P_{AA} = P_{BB} = l_i/L\,, \\ P_{AB} = P_{BA} = 1 - l_i/L\,. \end{cases} \tag{19}$$

To build a self-similar structure we allow l_{i_k} to scale as $l_{i_k}/L = (\frac{1}{2})^{V(i_k)}$, where $V(i_k)$ is a natural number sorted randomly for each site i_k ($i = -\infty$ to ∞, $k = A, B$). To deal with a real numerical experiment, we consider finite se-

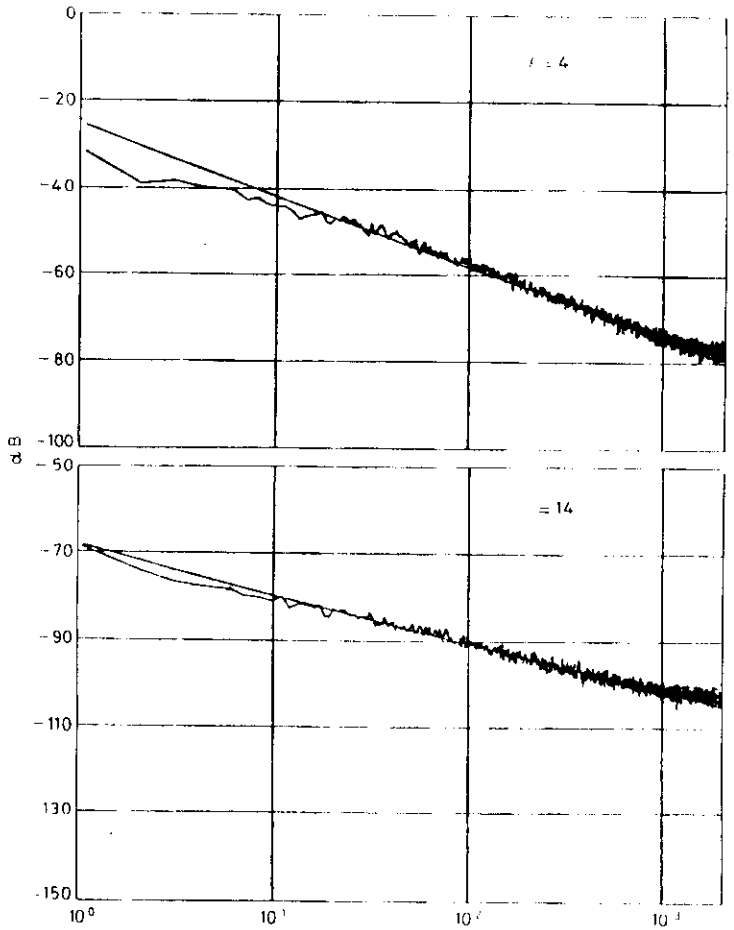

Fig. 18. – Power spectra (vertical) *vs.* frequency (horizontal) in double logarithmic scale. Wavy lines: measured spectra; straight lines: best fits, whose slopes α are reported in the next figure. The two samples shown refer to $F = 4$ and 14, respectively.

quences of N sites (*e.g.*, $N = 10^3$) and we truncate the fractality by imposing $0 \leq V(i_k) < F$. Here, F is a finite integer denoting the maximum partitioning $(\frac{1}{2})^{F-1}$, that is, the ultimate resolution of the measuring device in appreciating the fractal structure of our set. With all this in mind, for each evolution we extract a double sequence of N integers randomly distributed between 0 and $F-1$, and denote each site i_k by the corresponding number $V(i_k)$. This means that we have attributed to each site an «area of respect», that is, a specific separation l_{i_k} from the other attractor, with l_{i_k} depending on $V(i_k)$, as shown above. We start, *e.g.*, on the basin A from $i_A = N/2$.

At this step, to account for a suitable noise yielding the permanence and jump probabilities (19), we generate a random number y uniformly distributed between 0 and 1. If $y \leq (\frac{1}{2})^{V(i_A)}$, then at the next time the point goes to $i_A + 1$ on attractor A; if $y > (\frac{1}{2})^{V(i_A)}$, then the point jumps instantaneously to site i_B and at the next time it goes to $i_B - 1$ on attractor B.

By measuring the position co-ordinate, taking the Fourier transform and squaring it, we can build the power spectra, that is, the transforms of the position correlation functions.

In fig. 18 we show two power spectra for $F = 4$ and 14, respectively. In fact, we have measured spectra for all integer values of F between 4 and 14, but we just report two samples over slightly more than three frequency decades. The sequence shows that, as the fractality increases, the slope of the double logarithmic plot goes from about 2 (single Lorentzian) to about 1 ($1/f$ spectrum). This appears better in fig. 19, where the slope α of the $f^{-\alpha}$ spectral law is plotted

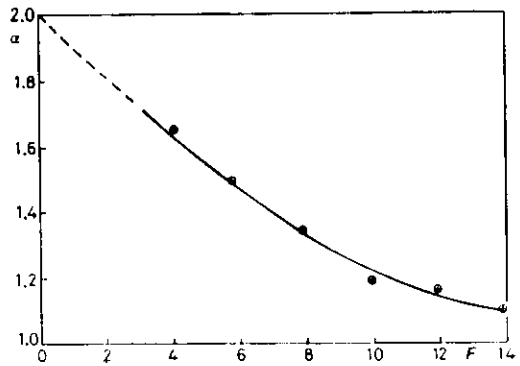

Fig. 19. – Exponents α of the power law $f^{-\alpha}$ *vs.* fractality F.

vs. the fractality F. The Lorentzian ($\alpha = 2$) of the random telegraph model is easily recovered for $F = 1$, thus showing that noise-induced jumps across a regular line boundary fulfil the intuitive expectation of a single decay rate. An analogy with the random-random walk [27, 28] is easily drawn. Indeed

our motion is bound with a r.m.s. deviation going from about $\sqrt{t}$ to $|\log t|^2$ as the fractality F increases from 4 to 14, according to SINAI.

For comparison we mention other approaches leading to $1/f$ or anyway non-Lorentzian low-frequency spectra:

i) Pomeau-Manneville type-3 intermittency corresponds to slowly diverging trajectories with a $1/f$ power spectrum [39]. This behaviour is intrinsic to the dynamics, hence it occurs without noise.

ii) A deterministic diffusion process may occur beyond «crisis» [40] when two otherwise disjoint attractors merge into a single one. Here again no noise is required, and a comparison of this behaviour with noise-induced jumps was given in ref. [35].

iii) Another comparison of intrinsic *vs.* noise-induced intermittency was carried on for a damped driven pendulum, which models a Josephson junction [41]. This last paper offers numerical evaluations of spectra, showing a $1/f$ region extending over two decades, but to our knowledge nobody has tried so far to analyse the role of fractality and draw a comparison with Sinai subdiffusive motion.

Among other things, the results of this paper may strongly affect our current understanding of optical-bistability (OB) phenomena. OB is described in terms of two fixed-point attractors, which, however, are the result of a collective dynamics implying many degrees of freedom. There are no exhaustive analyses of the structure of the basin boundary, thus possible fractal structures may appear if the dynamics is evaluated in detail. On the other hand, in order to reduce the signal power necessary to drive the OB device from one state to the other, the system is usually set very near to the boundary. Thus unavoidable random noise might induce low-frequency spectra of the type above described.

8. – Conclusion: long memory in statistical physics.

Let me conclude with a speculation on the role of the long-time terms in nonequilibrium statistical mechanics.

We have shown that, whenever in nonlinear dynamics more than one attractor is present, there are two distinct power spectra:

i) a high-frequency one, corresponding to the decay of correlations within one attractor;

ii) a low-frequency one, corresponding to noise-induced jumps.

Based upon i), the usual transport coefficients for macroscopic equations of evolution have been built. Effect ii) has been overlooked so far. Here, I wish to consider an example showing the relevance of ii) with respect to multiphoton molecular excitation.

Let me consider a molecule with two isomeric states (cis and trans) of almost equal energy, separated by an energy barrier, say, of 1 eV (*e.g.*, rhodopsin molecule in the retina of vertebrates).

We known that an IR laser such as a CO_2 laser ($\lambda = 10\ \mu m$, $h\nu \simeq 0.1$ eV) may give rise to a multiphoton absorption process if it is powerful enough to provide 10 photons within one coherence time of the «cis» valley, so that 10 small photons pile up to 1 eV excitation. (We are considering a molecule large enough so that the barrier is already a classical one, and so quantum tunnelling is possible.) We know that a vibrational mode IR active decays by intramolecular relaxations toward the thermal bath of all other modes, in a time of order of 10^{-12} s = 1 ps. In order to have a multiphoton isomeric transition, we should have a laser power of

$$10 \text{ photons/1 ps} \simeq 10^{-7} \text{ W}$$

over a cross-section of $\sim (1\ \text{Å})^2 = 10^{-16}\ \text{cm}^2$, and thus a laser intensity of 10^9 W/cm^2. But this was a Markovian point of view, based on a memory time of 1 ps related to the high-frequency spectral broadening. A double potential valley dynamics is described by a Duffing equation (see ref. [29, 35]) and the presence of an IR laser illumination as a forcing term yields a motion on an attractor not necessarily confined in one valley, even for very low intensities (see fig. 3 of ref. [29]).

Such a chaotic motion may pass near to the boundary, hence requiring an activation energy much less than the barrier of 1 eV to be introduced into an Arrhenius type law. For instance, in fig. 2 we have seen a high-frequency spectrum around 100 kHz, and in fig. 5 the corresponding low-frequency jump spectrum at 1 Hz (5 decades below). By the same reasoning, we might expect that an intensity 5 or 6 decades lower (that is, 10 photons/μs or just 10^3 W/cm) might be sufficient for a multiphoton isomerization process.

If we could use such a large enhancement factor in most activation processes of biochemical relevance, the consequence would be that the times necessary for biochemical evolution on Earth could be correspondingly reduced.

This is just a guess, to show how the introduction of the long-memory processes here described for the first time may open new routes in the physics of complex systems.

REFERENCES

[1] W. E. LAMB jr.: *Phys. Rev.* **134**, A 1429 (1964).
[2] H. HAKEN: *Laser theory*, in *Encyclopedia of Physics*, Vol. XXV/2c, edited by S. FLÜGGE (Springer Verlag, Berlin, 1970), p. 51.
[3] M. SCULLY and W. E. LAMB jr.: *Phys. Rev. Lett.*, **16**, 853 (1966); *Phys. Rev.*, **159**, 208 (1967); **166**, 246 (1968).

[4] J. P. GORDON: *Phys. Rev.*, **161**, 367 (1967).
[5] H. HAKEN: *Synergetics*, 3rd edition (Springer-Verlag, Berlin, 1983).
[6] F. T. ARECCHI: in *Order and Fluctuations in Equilibrium and Nonequilibrium Statistical Mechanics, Proceedings of the XVII Solvay Conference on Physics*, edited by G. NICOLIS *et al.* (J. Wiley, New York, N. Y., 1981), p. 107.
[7] R. J. GLAUBER: in *Quantum Optics and Electronics*, edited by C. DE WITT, A. BLANDIN and E. COHEN-TANNOUDJI (Gordon and Breach, London, 1965).
[8] F. T. ARECCHI: in *Quantum Optics, Proc. S.I.F.*, Corso XLII, edited by R. J. GLAUBER (Academic Press, New York, N. Y., 1969), p. 57.
[9] F. T. ARECCHI and R. G. HARRISON, Editors: *Instabilities and Chaos in Quantum Optics* (Springer-Verlag, Berlin, 1986).
[10] E. M. LORENZ: *J. Atmos. Sci.*, **20**, 130 (1963).
[11] J. P. ECKMANN: *Rev. Mod. Phys.*, **53**, 643 (1981); J. P. ECKMANN and D. RUELLE: *Rev. Mod. Phys.*, **57**, 617 (1985).
[12] F. T. ARECCHI, G. L. LIPPI, G. P. PUCCIONI and J. R. TREDICCE: *Opt. Commun.*, **51**, 308 (1984).
[13] F. T. ARECCHI, R. MEUCCI, G. P. PUCCIONI and J. R. TREDICCE: *Phys. Rev. Lett.*, **49**, 1217 (1982).
[14] G. L. LIPPI, J. R. TREDICCE, N. B. ABRAHAM and F. T. ARECCHI: *Opt. Commun.*, **53**, 129 (1985).
[15] F. T. ARECCHI, W. GADOMSKI and R. MEUCCI: *Phys. Rev. A*, **43**, 1617 (1986).
[16] J. D. FARMER: *Physica (Utrecht) D*, **4**, 366 (1982).
[17] B. B. MANDELBROT: *The Fractal Geometry of Nature* (Freeman, San Francisco, Cal., 1982).
[18] P. GRASSBERGER and I. PROCACCIA: *Phys. Rev. Lett.*, **50**, 346 (1983).
[19] G. P. PUCCIONI, A. POGGI, W. GADOMSKI, J. R. TREDICCE and F. T. ARECCHI: *Phys. Rev. Lett.*, **55**, 339 (1985).
[20] G. IOOS and D. D. JOSEPH: *Elementary Stability and Bifurcation Theory* (Springer-Verlag, Berlin, 1980).
[21] P. GRASSBERGER: *J. Stat. Phys.*, **26**, 173 (1981).
[22] J. R. TREDICCE, F. T. ARECCHI, G. L. LIPPI and G. P. PUCCIONI: *J. Opt. Soc. Am. B*, **2**, 173 (1985).
[23] J. L. BOULNOIS, P. COTTIN, A. VAN LENBERGHE, F. T. ARECCHI and G. P. PUCCIONI: *Opt. Commun.*, **58**, 124 (1986).
[24] L. LUGIATO, L. M. NARDUCCI, D. K. BANDY and C. A. PENNISE: *Opt. Commun.*, **46**, 64 (1983).
[25] D. K. BANDY, L. M. NARDUCCI and L. LUGIATO: *J. Opt. Soc. Am. B*, **2**, 248 (1985).
[26] F. T. ARECCHI and A. CALIFANO: *Europhys. Lett.*, **3**, 5 (1987).
[27] IA. G. SINAI: in *Proceedings of the Berlin Conference on Mathematical Problems in Theoretical Physics*, edited by R. S. SCHRADER *et al.* (Springer-Verlag, Berlin, 1982), p. 12.
[28] E. MARINARI, G. PARISI, D. RUELLE and P. WINDEY: *Phys. Rev. Lett.*, **50**, 1223 (1983).
[29] F. T. ARECCHI and F. LISI: *Phys. Rev. Lett.*, **49**, 94 (1982).
[30] P. DUTTA and P. M. HORN: *Rev. Mod. Phys.*, **53**, 497 (1981).
[31] R. F. MIRACKY, J. CLARKE and R. H. KOCH: *Phys. Rev. Lett.*, **50**, 856 (1983).
[32] R. L. KAUTZ: *J. Appl. Phys.*, **58**, 424 (1985).
[33] *a*) M. R. BEASLEY, D. D'HUMIERES and B. A. HUBERMAN: *Phys. Rev. Lett.*, **50**, 1328 (1983). *b*) R. VOSS: *Phys. Rev. Lett.*, **50**, 1329 (1983). *c*) F. T. ARECCHI and F. LISI: *Phys. Rev. Lett.*, **50**, 1330 (1983).
[34] F. T. ARECCHI, R. BADII and A. POLITI: *Phys. Rev. A*, **29**, 1006 (1984).

[35] *a*) F. T. ARECCHI, R. BADII and A. POLITI: *Phys. Lett. A*, **103**, 3 (1984). *b*) F. T. ARECCHI, R. BADII and A. POLITI: *Phys. Rev. A*, **32**, 402 (1985).
[36] E. W. MONTROLL and M. F. SHLESINGER: *Proc. Natl. Acad. Sci. USA*, **79**, 3380 (1982).
[37] F. T. ARECCHI and A. CALIFANO: *Phys. Lett. A*, **101**, 443 (1984).
[38] G. GREBOGI, E. OTT and J. A. YORKE: *Phys. Rev. Lett.*, **50**, 935 (1983); S. M. MCDONALD, C. GREBOGI, E. OTT and J. A. YORKE: *Physica (Utrecht) D*, **17**, 125 (1985).
[39] Y. POMEAU and P. MANNEVILLE: *Commun. Math. Phys.*, **74**, 189 (1980); I. PROCACCIA and H. SCHUSTER: *Phys. Rev. A*, **28**, 1210 (1983).
[40] T. GEISEL and S. THOMAE: *Phys. Rev. Lett.*, **52**, 1936 (1984); T. GEISEL, J. NIERWETBERG and A. ZACHERL: *Phys. Rev. Lett.*, **54**, 616 (1985).
[41] E. G. GWINN and R. M. WESTERVELT: *Phys. Rev. Lett.*, **54**, 1613 (1985).